



Partial hydrogenation of anisole to cyclohexanone in water medium catalyzed by atomically dispersed Pd anchored in the micropores of zeolite



Kaiyang Xu ^a, Yu Chen ^a, Hua Yang ^a, Yuyan Gan ^a, Lizhi Wu ^a, Li Tan ^a, Yihu Dai ^b, Yu Tang ^{a,*}, ¹

^a Institute of Molecular Catalysis and In-Situ/Operando Studies College of Chemistry, Fuzhou University, Fuzhou 350108, China

^b Institute of Advanced Synthesis, School of Chemistry and Molecular Engineering, Nanjing Tech University, Nanjing 211816, China

ARTICLE INFO

Keywords:
Biomass
Hydrogenation
Cyclohexanone
Palladium
Single atom catalyst

ABSTRACT

Cyclohexanone is an important raw material for manufacturing nylon and other chemicals. The sustainable conversion of biomass derived molecules to cyclohexanone is desired but still challenging. Herein, a palladium single atom catalyst anchored in the micropores of zeolite (namely Pd₁/ZSM-5) is designed and exhibits remarkable catalytic activity in transforming anisole to cyclohexanone in water medium (H₂O), without using of organic solvent or halogen promoter. The selectivity to cyclohexanone is 91.2% and the turnover rate (TOR) is 400.8 h⁻¹ at 453 K. The Pd sites, acid sites, and microporous confinement environment of zeolite cooperate to promote the partial hydrogenation to cyclohexanone, and inhibit further hydrogenation as the side reaction. H₂O not only acts as the solvent, but also participates significantly in the partial hydrogenation. Moreover, as revealed by isotope labelled experiments (D₂O and H₂¹⁸O), the water participated hydrogenolysis and the consequent partial hydrogenation mechanism is proposed.

1. Introduction

Cyclohexanone is one of those most important chemical raw materials, which is the intermediate for production of nylon, caprolactam, adipic acid and other substances [1]. The annual production of cyclohexanone was *ca.* 6.4 million tons in 2020, equivalent to about 7.8 billion US dollars. Currently, the industrial production of cyclohexanone consists primarily of the oxidation of cyclohexane or the hydrogenation of phenol, both of which significantly rely on the petroleum chemicals heavily [2,3]. The oxidation route has widely used in industrial production for its relatively low cost. However, this process produces byproducts such as cyclohexanol and organic acids that make separation difficult and typically result in a low yield of cyclohexanone [4,5]. In addition, the hydrogenation route has been developed in terms of one-step or two-step methods. The two-step method involves first step of hydrogenation of phenol to cyclohexanol, and then second step of dehydrogenation to cyclohexanone under a Cu/Zn catalyst [6]. Compared with other routes, the one-step process, or so called partial hydrogenation process, is attracting more and more attentions for its unique advantages such as mild reaction condition, thermal dynamics feasible, and facile product separation [7–10].

Utilization of biomass as raw materials to produce high value chemicals can effectively reduce the carbon dioxide emission. Lignin is one of the most promising renewable biomass sources for its abundance and relatively low cost [11,12]. Generally, lignin is composed of many aryl ether segments and rich in aryl ether bonds. These natural aromatic carbon-oxygen (C_{aryl}-O) bonds are potential candidates for directly conversion to ketones through partial hydrogenation of aromatic rings, however, which has not been fully developed yet. In recent years, many efforts have been made to develop effective solution to convert lignin-derived aromatic ethers into ketones [13,14]. The relative low selectivity to cyclohexanone among all hydrogenation products is one of the key challenges [15–19]. Recently, Meng et al. reported a bromide-modified Pd/C catalyst in the H₂O/CH₂Cl₂ medium for effectively inhibiting the side reactions during the partial hydrogenation of anisole, with the yield to cyclohexanone of 96% [20]. However, the usage of organic solvents and halogen promoters still brings concerns on the environmental hazard and further hampers the potential application. Therefore, developing an effective, high selective and environmentally friendly catalyst for partial hydrogenation of aromatic ethers is still desired.

Single-atom catalysts have been the frontier of the catalysis research

* Corresponding author.

E-mail address: yu.tang@fzu.edu.cn (Y. Tang).

¹ ORCID: 0000-0001-9435-9310

for its unique features in the recent decade, especially the singly dispersed transition metal catalysts confined in the pores of zeolites [21–25]. Atomically dispersed precious metal atoms anchored on the internal surface of micropores of zeolite could offer a distinctly different chemical state, and further exhibit a distinctly different catalytic activity [26–31]. Nevertheless, the shape-selective effect of the confined channel of zeolites can effectively reduce the occurrence of side reactions and improve the selectivity of the target product. Moreover, the isolated acid sites in the internal pores of zeolites can strongly anchor metal ions to form singly dispersed metal sites and adjacent acid sites, and further participate and promote the catalytic reaction [32,33].

In this work, we investigate a $\text{Pd}_1/\text{ZSM-5}$ catalyst containing single atom Pd sites as well as acid sites in the micropores. It is found that the $\text{Pd}_1/\text{ZSM-5}$ catalyst, with singly dispersed Pd_1O_4 sites anchored on the internal surface of micropores of ZSM-5, is highly efficient for the conversion of a biomass model molecule, anisole, to cyclohexanone in H_2O medium. The turnover rate is 400.8 h^{-1} and the selectivity is 91.2%, without any usage of organic solvent or halogen promoter at 453 K and 2 MPa. The Pd_1O_4 sites, confinement space of the micropores, and the acid sites of the zeolite are essential factors for the partial hydrogenation activity and high selectivity. Mechanism studies suggest H_2O not only acts the role of solvent but also directly participates in the catalytic hydrogenation of anisole. This work demonstrates the significance of the synergistic effect between catalytic sites in confined pores, and further explores the application in catalyzing biomass-derived molecules to cyclohexanone under mild and sustainable condition.

2. Experiments

2.1. Materials

$\text{Pd}(\text{NO}_2)_2 \bullet x\text{H}_2\text{O}$ and tert-butylboramine borane (BTBC) were purchased from Sigma-Aldrich. Anisole (AR, 99%), Cyclohexanol (AR, $\geq 98.5\%$), Dodecane (GC, 99.0%), Dichloromethane (GC, $\geq 99.9\%$), containing 50–150 ppm Isopentene), Phenol (AR, 99%), Cyclohexanone (AR, 99.0%), Cyclohexane (ACS, $\geq 99\%$), palladium acetylacetonate (AR, 99%), Oleylamine (C_{18} : 80–90%) were purchased from Aladdin Chemistry Co. Ltd, Shanghai. Ethyl acetate (AR, $> 99.5\%$), HNO_3 (AR), HCl (AR) were purchased from Sinopharma chemical reagent Co. Ltd. Decalin (95%) was used as received from Macklin. Benzene and HF (AR, $\geq 40\%$) were obtained from Xilong Scientific Co. LTD. H-ZSM-5, NaZSM-5, Beta zeolites were purchased from Nankai University Catalyst Co. Ltd. All materials were not further purified before using unless noted.

2.2. Synthesis of $\text{Pd}_1/\text{ZSM-5}$ catalyst

The $\text{Pd}_1/\text{ZSM-5}$ catalysts were synthesized by a modified incipient wet impregnation (IWI) method [27,28,31]. Commercial purchased ZSM-5 ($\text{Si}/\text{Al} = 27$) was calcined in air at 550 °C for 12 h to remove template. Before IWI, the pore volume of ZSM-5 was measured. Firstly, 2.0 g ZSM-5 zeolite particles were dried at 100 °C for 1 h. Secondly, a solution of palladium nitrate with a volume equal to the pore volume of 2 g ZSM-5 was prepared. The concentration of Pd is dependent on the nominal loading of Pd for the desired catalyst. Thirdly, the solution of Pd was introduced to the ZSM-5 powder drop by drop at a rate of 0.2 ml/min. During the impregnation, the ZSM-5 was kept to under stirring. The resulting products were aged for 2 h before drying. Finally, it was dried at 80 °C overnight and calcined in air at 450 °C for 4 h with a ramping speed of 2 °C per minutes. Pd_1/Beta and $\text{Pd}_1/\text{NaZSM-5}$ were synthesized with the same method as $\text{Pd}_1/\text{ZSM-5}$.

2.3. Synthesis of $\text{PdNP}/\text{ZSM-5}$ catalyst

For a typical synthesis of PdNP, 150 mg of palladium acetylacetonate was added to 30 ml of oleylamine and stirred at 60 °C until dissolved [34]. Then 260 mg BTBC (tert-butylboramine borane) was put in at one

time, and the solution quickly changed from light yellow to dark black. Next, the temperature was raised to 90 °C and kept for 1 h under stirring, and then cooled to room temperature under stirring. Then, the twice volume of ethanol was added for precipitation. After centrifugation, a black solid was obtained, which was washed and dried by ethanol and dispersed in toluene. Finally, 1 g dried HZSM-5 was added to the above toluene solution and kept stirring for 10 min, followed by drying at 80 °C overnight and calcined in 5% H_2/Ar at 550 °C for 4 h with a ramping speed of 2 °C per minute [35].

2.4. Catalytic test

Partial hydrogenation of anisole was performed in a high pressure batch reactor with a thermal couple installed on the reactor and dipped into the reactants to monitor the temperature. The reactants were stirred and heated during reaction. A typical procedure was as follows: 200 mg catalyst, 0.6 ml anisole (5.54 mmol), 100 μL dodecane (the internal standard), 15 ml H_2O were placed in the glass beaker. The reactor was sealed and charged with H_2 of the initial pressure of 2 MPa after purging by four times. Then, the reactor was kept at 180 °C for 3 h with a stirring rate of 800 rpm. After reaction, the reactor was placed in the flowing cold water to quench the reaction and the products were extracted by ethyl acetate. The extract liquid was centrifuged and then analyzed by GC-MS (Shimazu, GCMS-QP2010SE) equipped with a capillary column (Rtx-5MS, 30 m in length, 0.25 mm in inner diameter, 0.25 μm in film thickness). The gas phase product was analyzed by a GC-2014 (Shimazu, Japan) equipped with a FID detector.

2.5. Characterization

X-ray diffraction measurements were conducted on an X-ray diffractometer (Smart Lab SE, Rigaku) operated at 40 kV and 40 mA with $\text{Cu K}\alpha$ ($\lambda = 0.154 \text{ nm}$) radiation. The range of 2θ was between 5° and 90°. Step width was 0.02° with the speed at 5°/min.

TEM images were measured on a FEI Talos F200S G2 operating at 200 kV. Before testing, the sample was fully ground in agate mortar and dispersed in the ethanol by ultrasound for 0.5 h, then one or two drops were impregnated into the carbon film micro-grid copper net and natural drying for 12 h.

The authentic loading amount of Pd in catalysts was determined by Inductively Coupled Plasma-Optic Emission Spectroscopy techniques (iCAP 7000 SERIES, Thermo Scientific). In a typical procedure to dissolve Pd, 50 mg catalyst was placed in a Teflon-lined stainless steel autoclave, following by addition of 1 g H_2O and 1 g HF. The mixture was aged for 3 h and 4 g aqua regia was introduced before hydrothermally treating at 80 °C for 24 h.

X-ray absorption spectrum of Pd K edge was collected under fluorescence mode with a Ge solid state multi-channel detector. A piece of Pd foil was placed between detector I_1 and I_2 , then its spectrum was recorded accompanied with the sample for energy alignment. XAS data was processed and fitted with ARTEMIS and ATHENA software [36]. The K-edge spectrum of a metallic Pd foil was collected at the same time for the evaluation of S_0^2 for data fitting. The coordination umber (CN), distance and Debye-Waller factor (σ^2) were set as fitting parameters. All the FT-EXAFS spectra are presented without phase correction. The amplitude of the Fourier transformed spectra of EXAFS of Pd foil is rescaled by 0.5 for better comparison in Fig. 2.

The FTIR spectra were recorded with a Nicolet iS50 spectrometer (Thermo-Fisher, USA) equipped with an attenuated total reflection (ATR) detector. In the anisole adsorption test, the potassium bromide was fully ground before pelleting, following by dropping 100 μL anisole into the tablet and baking for 0.5 h under the infrared lamp. Then the IR spectra of anisole was collected by transmission mode. As for the IR spectrum of catalysts adsorbed anisole, 50 mg catalysts were pretreated with 100 μL anisole at 70 °C for 12 h under vacuum, and then the IR spectra were collected by the ATR mode.

3. Results and discussions

3.1. Design and characterization of the Pd single atomic catalytic sites in the micropores

The catalyst is designed based on following considerations. The isolated Brønsted acid sites (BAS) in the internal pores of zeolites can not only effectively adsorb and activate the aromatic carbon-oxygen bonds [37], but also offer the sites to anchor the transition metals [28,31]. In general, H₂ can be activated on the surface of transition metals or single atomically dispersed metal cations [38]. Among those catalytic active transition metals, Pd is chosen in the catalyst design for the superior hydrogenation activity of Pd and unique performance of Pd single atom catalyst [1,3]. Hence, a series of zeolites supported Pd catalysts were prepared via a modified impregnation method (see the Section 2 and the Supplementary Information) [27,28,31]. A few typical zeolites, including H-ZSM-5, Na-ZSM-5 and Beta were investigated as the supports. The porosity properties of the zeolites were measured by N₂ adsorption-desorption as summarized in Table S1. The pore channels and size parameters of the zeolite supports are summarized in Table S2. The major differences among the zeolites are the acid sites and the maximum molecules size allowed to enter the pores. ZSM-5 and Beta is belonged to the MFI and BEA type of zeolite, respectively. They are featured with different three-dimensional pore structures. The pore size of ZSM-5 is similar to that of anisole, while the pore size of Beta is much larger than that of anisole. The synthesized catalysts are Pd₁/ZSM-5, Pd₁/NaZSM-5, Pd₁/Beta and PdNP/ZSM-5. The authentic loading concentration of Pd in the catalysts were examined by Inductive Coupled Plasma Optic Emission Spectrum (ICP-OES) in Table S3, which is 0.028%, 0.037%, 0.035%, and 1.9%, respectively. The acidity of the catalysts was tested by NH₃-TPD (Figure S1). The Pd₁/ZSM-5 and Pd₁/Beta exhibit a typical acidity pattern, which are Lewis acid and Brønsted acid, respectively. However, the Pd₁/NaZSM-5 only presents the pattern of the Lewis acid, suggesting lacking of Brønsted acid sites (BAS) compared with the Pd₁/ZSM-5 catalyst.

The crystal structure of the Pd₁/zeolite catalyst was evaluated by XRD as shown in Figure S2. No characteristic peaks of Pd particles or palladium oxide are observed. Besides, the used Pd₁/ZSM-5 retains the diffraction peaks of MFI zeolite after reaction, indicating the Pd₁/ZSM-5 catalyst is stable after reaction. In the similar manner, Pd₁/Beta and Pd₁/NaZSM-5 also show their own characteristic diffraction patterns of zeolite only (Figure S2b). On the contrary, the formation of Pd nanoparticles for PdNP/ZSM-5 was proofed by XRD (Figure S3) and transmission electron microscopy (Figure S4). The diffraction peaks at 40.0° and 46.6° in the XRD patterns can be assigned to the (111) and (200) planes of metal palladium particles, respectively [27,34,35,39]. The TEM images of PdNP/ZSM-5 reveal well-dispersed Pd particles with a mean size of 9.0 nm (Figure S4).

The Pd₁/ZSM-5 catalyst was further investigated by transmission electron microscopy (TEM) as shown in Fig. 1. There are only ZSM-5 nanoparticles observed (Fig. 1a) without observation of Pd or PdO nanoparticles on the zeolite under bright field image, excluding the formation of Pd or PdO nanoparticles. In order to further investigate the status of Pd, the high-angle annular dark-field (HAADF) image of a catalyst nanoparticle and corresponding elements mapping of Pd and Al were captured in Fig. 1b. Clearly, both Pd and Al are uniform-dispersed in the catalyst. The results from TEM study show that Pd species are highly dispersed in the zeolite. This observation is consistent with those isolated metal cations anchored in the micropores of zeolite as the single atom catalysts, where the Al sites in the framework of zeolites play the key role to anchor and stabilize the metal cations [27, 28, 31, 40–42].

X-ray absorption spectroscopic studies, including near-edge X-ray absorption fine structure (XANES) and extended X-ray absorption fine structure (EXAFS), were performed to further study the electronic state and local coordination environment of Pd species in the catalyst. The full spectra and XANES of Pd K-edge for Pd₁/ZSM-5 are summarized in Fig. 2a-b with the comparison with Pd foil and PdO references. The edge energy and edge height of Pd₁/ZSM-5 are closed to that of PdO, indicating that the electronic state and chemical state of Pd in Pd₁/ZSM-5 are close to that of PdO. In other words, the Pd atoms in Pd₁/ZSM-5 are in cationic state. Moreover, Fourier-transformed (FT) EXAFS spectra of Pd K-edge for Pd₁/ZSM-5, PdO and Pd foil are demonstrated in Fig. 2c and S5. All the Fourier-transformed EXAFS spectra are plotted without phase correction. There is one major peak observed at ~1.5 Å, which is assigned to oxygen atoms coordinated with the Pd atom. There is lacking of Pd-Pd bond of Pd particles at ~2.5 Å, or Pd-O-Pd bond of PdO at ~3.0 Å [27]. Besides, DRIFT-CO results also support this standpoint (Figure S6). It's observed that the Pd₁/ZSM-5 and Pd₁/ZSM-5 after regeneration both show a peak of 2140 cm⁻¹, which can be attributed to the linear absorption of CO on the single atom Pd [28,41,43]. The bridge adsorbed CO on continuous Pd-Pd sites (~1933 cm⁻¹) is not found in the DRIFT-CO spectrum. This not only indicates that the Pd is singly dispersed, but also can maintain the singly dispersed state after reaction. Furthermore, the data fitting and corresponding fitting parameters of Pd₁/ZSM-5 are summarized in Fig. (2d, e). The coordination number (CN), distance and Debye-Waller factor were set as fitting variables. The coordination number (CN) of Pd-O pathway of Pd₁/ZSM-5 is 3.74 ± 0.32, suggesting the configuration of single Pd atom is Pd₁O₄. The Pd is anchored to Brønsted acid sites (BAS) instead of entering the framework of zeolite [23,27,28,40]. A coordination model of Pd₁O₄ in Pd₁/ZSM-5 is shown in the inset image of Fig. 2d, with Pd in green, O in red, Si in yellow and H in white. Three oxygen atoms are attributed to the oxygen atoms in the internal wall of micropores of zeolite, while another one is assigned to hydroxyl group on Pd. Therefore, the catalyst is referred as Pd₁/ZSM-5, Pd₁O₄ and Pd/ZSM-5 interchangeably in the manuscript.

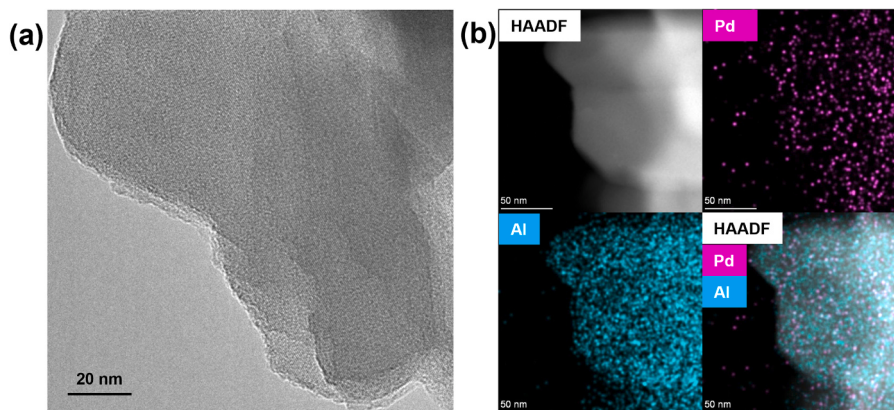


Fig. 1. Characterization of Pd₁/ZSM-5. (a) TEM image, (b) element mapping of Pd and Al sites, as well as HAADF image.

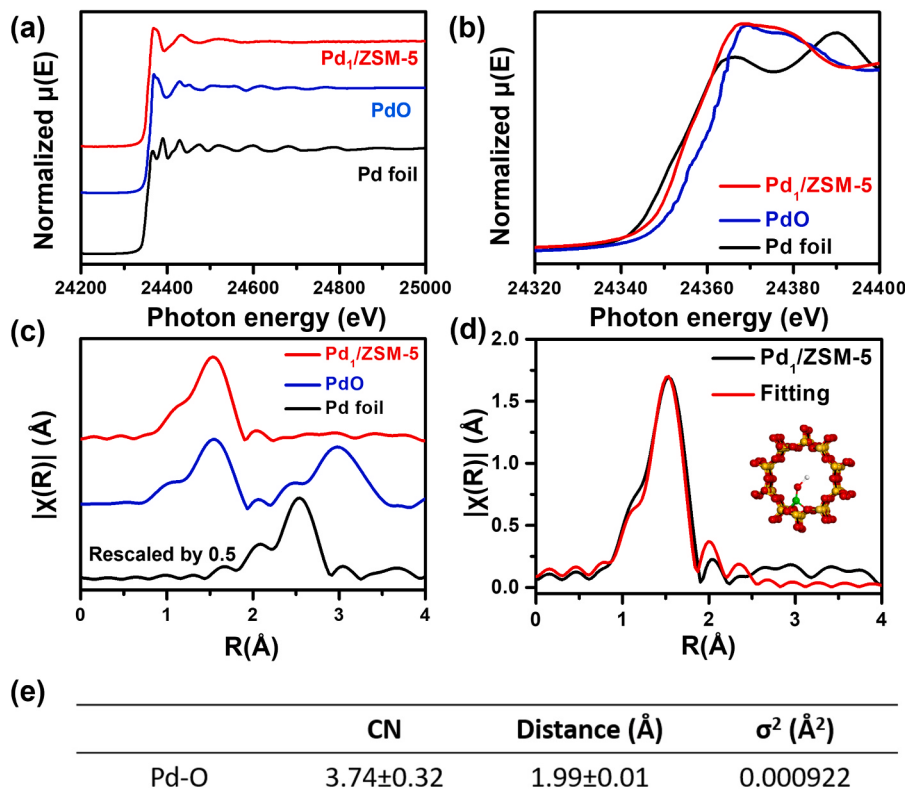


Fig. 2. XAS spectra of Pd K edge for Pd₁/ZSM-5. (a) the X-ray absorption spectra, (b) XANES of Pd K edge, (c) Fourier-transformed EXAFS spectra, and (d) data fitting for Pd₁/ZSM-5. (e) fitting parameters for Pd₁/ZSM-5. The Pd foil and PdO references are compared in the figures. The Fourier transformed spectra are plotted without phase correction. The amplitude of Fourier-transformed EXAFS spectrum Pd foil is rescaled by 0.5 for better comparison. The color code in the inset of (d): Pd in green, O in red, Si in yellow and H in white.

3.2. Partial hydrogenation activity of anisole to cyclohexanone on Pd₁/ZSM-5 catalyst

The catalytic performances of partial hydrogenation of anisole to cyclohexanone by various Pd-zeolite catalysts were investigated in a high pressure batch reactor. The evaluation of catalytic performance for all single atom Pd catalysts was calculated by the formulas shown at [supporting information](#). The intrinsic activity of catalysts is discussed in terms of turnover rate (TOR) to cyclohexanone under the conversion is less than 25% to ensure reaction rate is in the kinetic controlled regime. The mass transfer is discussed in [Supplementary Note 2](#). The catalytic key results are compared in [Table 1](#).

First of all, the HZSM-5 shows negligible catalytic activity as the control experiment in entry 5 of [Table 1](#). The minor conversion of

anisole is only 0.37%, and the product is phenol. This can be due to the hydrolysis of carbon-oxygen (C_{alkyl}-O) over BAS (See the [Supplementary Note 3](#)). Secondly, Pd₁/ZSM-5 exhibits a TOR of $400.8 \pm 30.1 \text{ h}^{-1}$, while the selectivity to cyclohexanone of $91.2 \pm 1.8\%$ for the reaction of partial hydrogenation of anisole. This is a remarkable activity and selectivity compared with other catalysts and results in literatures (see the discussion later) [15,16,20]. Thirdly, the catalytic performance of Pd₁/NaZSM-5 catalyst was examined to study the effect of BAS in zeolite under the same condition. Unfortunately, Pd₁/NaZSM-5 shows no catalytic activity for hydrogenation of anisole at all (entry 2 of [Table 1](#)), which demonstrates the presence of BAS is necessary for the reaction. The fourth, to identify the active sites of Pd₁/ZSM-5, the Pd nanoparticles (PdNP) supported on ZSM-5 was synthesized by deposition of colloid nanoparticles on support [34,35,44]. The obtained PdNP/ZSM-5 can be also confirmed by DRIFT-CO ([Figure S6](#)). The adsorbed band at 1933 cm^{-1} is attributed to the adsorption of CO on Pd nanoparticles. However, when the similar amount of Pd was used as the catalyst, none of catalytic activity was found as shown by entry 4 of [Table 1](#), indicating isolated Pd active sites are responsible for distinct catalytic performance instead of Pd particles (See the [Supplementary Note 1](#)). Finally, the Pd₁/Beta catalyst was evaluated to unveil the role of the pore size and structure of the zeolite. As shown in the [Table S2](#), the molecules can diffuse into the pore of a MFI structure is $4.46 \times 4.46 \times 4.7 \text{ Å}$, while is $5.95 \times 5.95 \times 5.95 \text{ Å}$ for BEA zeolite. Thus, the beta zeolite has larger capacity for reactant molecules to diffuse into. The TOR of Pd₁/Beta catalyst achieves a slight enhancement with $439.4 \pm 72.5 \text{ h}^{-1}$, which could be attributed to the feasible diffusion for anisole molecules into active sites inside the micropores. However, the selectivity to cyclohexanone over Pd₁/Beta decreases sharply to $67.0 \pm 6.3\%$. The by-product obtained from Pd₁/Beta catalyst is the coupling products of two cyclohexanone, indicating that the appropriate types and sizes of pore are also pivotal for partial hydrogenation of anisole. This result is in line with a recent literature. [45] As a brief summary, the high TOR and high selectivity are attributed to the integration of single atom dispersed Pd sites as Pd₁O₄, Brønsted acid sites and MFI pore structure in the

Table 1
Catalytic partial hydrogenation of anisole to cyclohexanone on Pd/zeolite catalysts.

Entry	Catalyst	Selectivity of cyclohexanone (%)	Turnover rate (TOR) ^{[d][h]} (h ⁻¹)
1 ^[a]	Pd ₁ /ZSM-5	$91.2 \pm 1.8^{[e]}$	400.8 ± 30.1
2 ^[b]	Pd ₁ /NaZSM-5	N.A.	N.A.
3 ^[b]	Pd ₁ /Beta	67.0 ± 6.3	439.4 ± 72.5
4 ^[c]	PdNP/ZSM-5 ^[f]	N.A. ^[g]	N. A.
5 ^[b]	H-ZSM-5 ^[f]	N.A.	N. A.

Notes: [a] 5.54 mmol anisole in 15 ml H₂O, 200 mg catalyst, 180 °C, 3 h, 2 MPa H₂. [b] 2.77 mmol anisole in 15 ml H₂O, 100 mg catalyst, 180 °C, 3 h, 2 MPa H₂. [c] 2.77 mmol anisole in 15 ml H₂O, 10 mg catalyst, 180 °C, 3 h, 2 MPa H₂. [d] Turnover rate (TOR) is defined as reaction rate to produce cyclohexanone molecules per Pd site per hr. Conversion is less than 25% to ensure the TOR is kinetic controlled. [e] The by product is cyclohexane. [f] A minor conversion of anisole is found as 0.37%. The product is phenol. [g] see the discussion in [Supplementary Note 1](#). [h] see the mass transfer evaluation in [Supplementary Note 2](#).

Pd₁/ZSM-5 catalyst. All the three factors are essential for the partial hydrogenation activity.

The catalytic performance of Pd₁/ZSM-5 in this work is compared with the catalysts reported in literatures (Table S4) [16,20]. Meng et al. reported a bromide-modified 5% Pd/C catalyst in the H₂O/CH₂Cl₂ medium for hydrogenation of anisole with a selectivity of cyclohexanone of 97%. However, the TOR is only 61.9 h⁻¹ and the usage of organic solvents and halogen salts hampers the potential application. Besides, Wang et al. studied the hydrogenation of diphenyl ether over 0.2% Pd/C catalyst in H₂O. It is found that the TOR is as high as 531.9 h⁻¹ but the selectivity of cyclohexanone is only 24.7% and the required temperature is 190 °C. Thus, in comparison with catalysts in literatures, the hydrogenation of anisole over Pd₁/ZSM-5 in H₂O under mild condition exhibits remarkable performance with the selectivity of 91.2% and the TOR of 400.1 h⁻¹.

The reaction parameters are optimized as shown in Fig. 3. Every controlled experiment is repeated at least three times to get the error bars. First of all, the TOR increases with the increasing of reaction temperature (Fig. 3a). However, the selectivity of cyclohexanone shows a slight decline but remains above 90% under all temperatures. Typically, the optimal TOR is obtained with 400.8 ± 30.1 h⁻¹ at 180 °C. Thus, the optimal temperature for partial hydrogenation of anisole is 180 °C. Secondly, the initial H₂ pressure charged into the reactor was optimized (Fig. 3b). With the increasing H₂ pressure, the TOR also increases rapidly and the selectivity remains above 90%. The optimal H₂ pressure was found to be 2 MPa. Moreover, variation of the dose of anisole shows minimum effect on the TOR, as shown in Fig. 3c. With the dose of anisole changes from 0.3 ml to 1 ml in a special experiment, the selectivity decreases gradually but keeps approximately 90% and the TOR remains with value from 368.2 h⁻¹ to 400.8 h⁻¹. It shows that the reaction has no mass transfer effect for anisole. In other words, this is a proof that the reaction is within kinetic controlled regime (See Supplementary Note S2). Nevertheless, with the low loading concentration of Pd as shown in Figure S16, the TORs are consistent among the Pd/ZSM-5 catalysts with the loading concentration of 0.028–0.099 wt%, suggesting the isolated Pd sites in HZSM-5 contribute to the partial hydrogenation. In summary, the optimal parameters of reaction are adjusted with 180 °C and 2 MPa.

The investigation on solvent effect is carried out by solvent screening (Figure S7). Protic solvents, including H₂O and ethanol, polar but aprotic solvents, including ethyl acetate and toluene, weak polar solvents, including decalin and trichloromethane are employed as the solvent for the hydrogenation of anisole. The reaction in pure H₂O shows the highest TOR and distinct selectivity for cyclohexanone over Pd₁/ZSM-5. In the case of pure alcohol, which belongs to protic solvent as well, no catalytic activity is observed. In fact, neither the polar aprotic solvents, nor the weak polar ones can be employed as solvent for hydrogenation of anisole on Pd₁/ZSM-5 for the reasons of their poor catalytic activity. Therefore, we can conclude that the partial

hydrogenation of anisole only can be conducted in H₂O, which highly implies H₂O could be a crucial role in the reaction pathway.

The kinetic analysis of Pd₁/ZSM-5 for partial hydrogenation of anisole are summarized in Fig. 4. The apparent activation barrier of partial hydrogenation of anisole is determined by Arrhenius equation ($k = Ae^{\frac{-Ea}{RT}}$, k is the apparent rate constant. A is pre-exponential factor. Ea is apparent activation barrier.). To an approximation, the rate constant is approximately proportion to the reaction rate when the conversion is low [46,47]. Then the apparent activation energy barrier of partial hydrogenation of anisole is determined by Arrhenius plots of Pd₁/ZSM-5 with 61.1 kJ·mol⁻¹. In addition, the apparent reaction order of H₂ and anisole is 1.6 and 0, respectively, indicating the H₂ pressure is a vital factor for hydrogenation reaction but the concentration of anisole is not. Interestingly, the reaction orders of H₂O is 1.7. It also implicates that H₂O may be another dominant factor for reaction kinetics. The apparent rate equation of this equation could be written as $TOR = k^*(P_{H_2}/P_0)^{\alpha}*[anisole]^{\beta}*[H_2O]^{\gamma}$, whereas the apparent rate constant (k) calculated by rate equation is 0.00355 h⁻¹, $\alpha = 1.62$, $\beta = 0$, and $\gamma = 1.70$. Taking the similarity of the reaction order of H₂ and H₂O (1.62 and 1.70, respectively) by Pd₁/ZSM-5, it is proposed the hydrogen transfer is coupled with the water molecule, which can act as an H-shuttling mediator that helps to transfer H from the catalyst surface to the reactants by solvation with proton [48–53]. This water-assisted hydrogen transfer mechanism has been proposed that H₃O⁺ is formed from the dissociation of H₂ and the solvation of H₂O, and then migrates this H to the reaction substrate [51,53]. In contrast, the apparent reaction order of H₂ and H₂O on PdNP/ZSM-5 catalyst is 1.56 and 1.09, respectively (Figure S14). The distinct reaction orders over Pd₁/ZSM-5 and PdNP/ZSM-5 suggest the reaction pathways are different.

The recycling experiments were carried out to investigate the stability and reusability of Pd₁/ZSM-5 catalysts. The catalyst was recovered simply by centrifuging, followed by drying at 80 °C and calcined in air at 350 °C for 4 h. As shown in Figure S8, a slightly decay in TOR was observed. Approximate 75% of initial activity remains well after 5 reaction cycle. This can be attributed to the loss of a few unstable single atom Pd under catalytic conditions and the remaining ones that are relatively stable would be responsible for the remained activity [23]. Nevertheless, the Pd₁/ZSM-5 catalyst also shows good performance on the time of stream in Figure S9. The conversion increases gradually and the selectivity remained at above 90% as the time of reaction increases. When the reaction proceeds for 24 h, the conversion eventually reaches 69.9 ± 3.9% and the selectivity is 92.0 ± 3.3%. The best catalytic performance of partial hydrogenation of anisole is 98.4% in conversion and 92.6% in selectivity under 12 h for reaction (Entry 3 of Table 2). Above all catalytic results demonstrate that the remarkable catalytic performance of Pd₁/ZSM-5 under a mild condition.

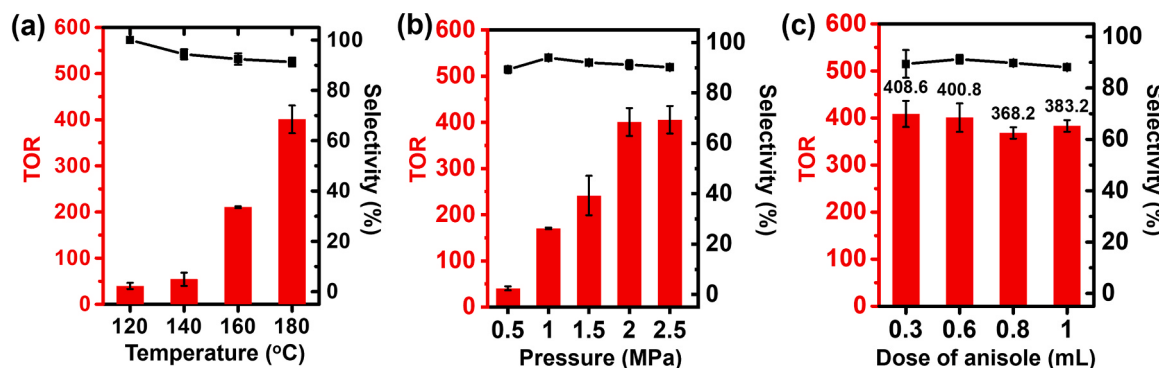


Fig. 3. Catalytic performance of Pd₁/ZSM-5 for selective hydrogenation of anisole to cyclohexanone. The turnover rate (TOR, h⁻¹) and selectivity to cyclohexane as the function of (a) reaction temperature, (b) initial H₂ pressure, and (c) usage of anisole. The general condition: 200 mg catalyst, 180 °C, 2 MPa, and 0.6 ml anisole.

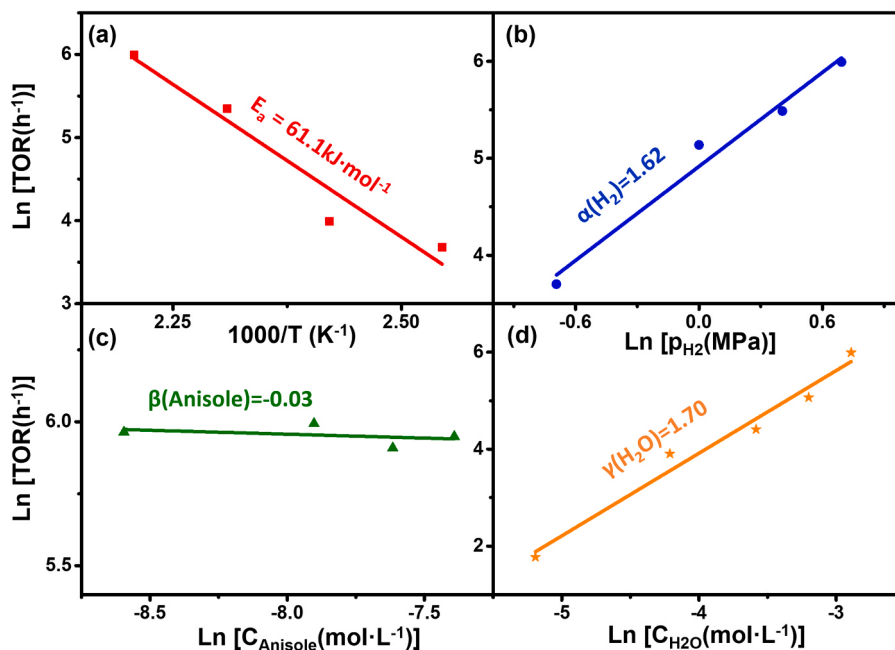


Fig. 4. Kinetic measurement of Pd₁/ZSM-5. (a) Arrhenius plots of Pd₁/ZSM-5 catalyzed-hydrogenation of anisole, and reaction orders of (b) H₂, (c) anisole, (d) H₂O for the apparent rate equation.

Table 2
Catalytic results for control experiments.

Entry	Reactant	Catalyst	Conversion (%)	Selectivity of cyclohexanone (%)
1 ^a	Cyclohexanone	HZSM-5	N.A.	N.A.
2 ^a	Cyclohexanone	Pd ₁ /ZSM-5	1.6 ^c	N.A.
3 ^b	Anisole	Pd ₁ /ZSM-5	98.4	92.6

^a 2.77 mmol cyclohexanone in 15 ml H₂O, 100 mg catalyst, 180 °C, 3 h, 2 MPa H₂.

^b 2.77 mmol anisole in 15 ml H₂O, 300 mg catalyst, 180 °C, 12 h, 2 MPa H₂.

^c cyclohexane is the major product.

3.3. The origination of high selectivity and activity in partial hydrogenation

From the fundamental aspect of view, catalysis on the surface of a solid catalyst starts from the adsorption of the reactant molecule(s). [54] Then, the adsorbed reactant molecule(s) on surface would be activated to participate the surface reaction(s) to form the intermediate and until the product molecule(s). The product molecule(s) desorbs from the surface of the catalyst to finish the reaction. To design a catalyst with high TOR and selectivity to a partial hydrogenation product, the catalytic site is expected to be highly specific to adsorb and activate the reactant molecules. Meanwhile, the desorption of the desired product molecule is also expected to be facile (Sabatier phenomenon) [55]. In other word, the catalytic sites are not active for the further consequence reaction(s) of the desired product molecule.

In this work, a unique feature of this Pd₁/ZSM-5 catalyst is the unexpected high selectivity to cyclohexanone, even in the case of long reaction time and high anisole conversion. For example, the selectivity is 92.6% when the conversion of anisole is 98.4% (Entry 3 of Table 2). It's well known that the product, cyclohexanone, can be further hydrogenated to cyclohexanol under the Pd nanoparticle catalysts [1,20,56,57]. To explain the distinct selectivity to cyclohexanone over Pd₁/ZSM-5 in partial hydrogenation of anisole, one control experiment is conducted over Pd₁/ZSM-5 under the same condition but using cyclohexanone as

the reactant. The catalytic results are listed at Table 2. For comparison, the ZSM-5 is inert for reaction. Interestingly, the Pd₁/ZSM-5 displays no catalytic activity in hydrogenation of cyclohexanone, suggesting the cyclohexanone could not further hydrogenate into cyclohexanol under the reaction condition. Moreover, considering the major side product is cyclohexane rather than methoxylcyclohexane (Table 1), the reaction mechanism on Pd₁/ZSM-5 catalyst is expected to be different from that of the consequential or compleptive hydrogenation pathways [9,16,58]. Thus, the research on the reaction mechanism starts from the absorption and desorption of reactant or product molecules on catalysts.

The anisole adsorbed on catalysts were firstly studied by Fourier-transformed infrared spectrum (FT-IR). As shown in Fig. 5a, the FT-IR spectrum of pure anisole and anisole adsorbed on different catalysts are compared. In a typical IR spectrum of free standing anisole, the C-O-C stretching vibration of aromatic ether is at 1040 cm⁻¹ [59,60]. It's observed that, when anisole is adsorbed on ZSM-5 or Pd₁/ZSM-5 catalyst, the vibration band of C-O-C downshifts from 1040 cm⁻¹ to 1035 cm⁻¹ and 1025 cm⁻¹, respectively, demonstrating the vibration energy of C-O-C bond of aromatic ether decreases when anisole is adsorbed on ZSM-5 or Pd₁/ZSM-5. On the contrary, the vibration band of C-O-C bond shift up from 1040 cm⁻¹ to, 1046 cm⁻¹, 1047 cm⁻¹, respectively, when anisole adsorbed on NaZSM-5 and Pd₁/NaZSM-5. The upshift of the vibration band indicates the increasing of the vibration energy of C-O-C bond, which may due the confinement from the framework of zeolites. The increasing of the C-O-C bond vibration energy would further increase the barrier for breaking of C-O-C bond, which is not favored for the reaction. Obviously, the difference of the adsorption properties of catalysts for anisole could attribute to the BAS of ZSM-5. Therefore, it is rational that Pd₁/ZSM-5 possesses the highest TOR for hydrogenation of anisole among all catalysts.

UV-Vis diffuse-reflectance spectrum (UV-Vis DRS) further suggests that anisole can be adsorbed on Pd₁/ZSM-5 with the BAS. As shown in Fig. 5b, the black line is the DRS of Pd₁/ZSM-5 and it can be seen that Pd₁/ZSM-5 spectrum displays weak bands in the region of ca. 460 nm that can be attributed to Pd d-d transitions and at ca. 280 nm due to the metal-oxygen charge transfer [61–64]. Immediately after adsorbing anisole on Pd₁/ZSM-5, a color change into pink was observed (see the

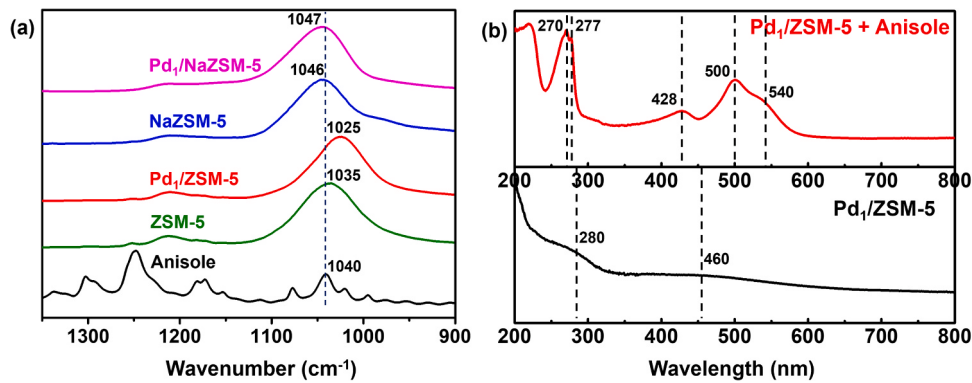


Fig. 5. Vibrational and electronic spectrum for anisole adsorbed on different catalyst. (a) FT-IR spectra and (b) UV-Vis DRS spectra of $\text{Pd}_1/\text{ZSM-5}$ catalyst with and without adsorbed anisole.

color change images in the Figure S12). That is also reflected in the spectrum with the red line in the top panel. The band at 270 nm and 277 nm can be assigned to the free standing anisole [65]. and the bands at 428 nm and 500 nm with a shoulder peak at 540 nm are contributed to the adsorbed anisole. In addition, the DRS of other reference catalysts adsorbed anisole are shown in the Figure S10. It is obvious that a broad absorption peak at 500 nm is obvious only when anisole is adsorbed on the Beta with BAS. At this stage, we can conclude that the anisole indeed can be adsorbed on the BAS of $\text{Pd}_1/\text{ZSM-5}$.

Therefore, The FTIR and UV-Vis spectrum studies suggest that the C–O bond of anisole can be selectively adsorbed and activated by the BAS of the internal surface of microporous of $\text{Pd}_1/\text{ZSM-5}$. At this stage, we can conclude that the singly dispersed Pd_1O_4 and BAS collaborate in the micropores to catalyze the partial hydrogenation of anisole.

3.4. The role of water revealed by isotope labeled experiments by using D_2O and H_2^{18}O

In order to further investigate the reaction mechanism, the isotope tracing experiments using isotope labeled reactants, such as D_2O and H_2^{18}O were performed. Due to the observation of small amount of phenol in the products by GC-MS, we suspect that phenol may be an intermediate for the reaction. Typically, the intensity of the mass-to-charge ratio (m/z) of 95 is 6.56% of that of $m/z = 94$ in a standard mass spectra of phenol (Fig. 6a). The $m/z = 95$ signal is attributed to the natural abundance of deuterium in phenol. In the experiment of using D_2O as the replaced solvent, 5 ml D_2O and 10 ml H_2O was mixed and used as solvent. The intensity of $m/z = 95$ is 138% of $m/z = 94$ (Fig. 6b), indicating that the accumulation of deuterium replaced phenol during the reaction. Additionally, two control experiments were designed to exclude the

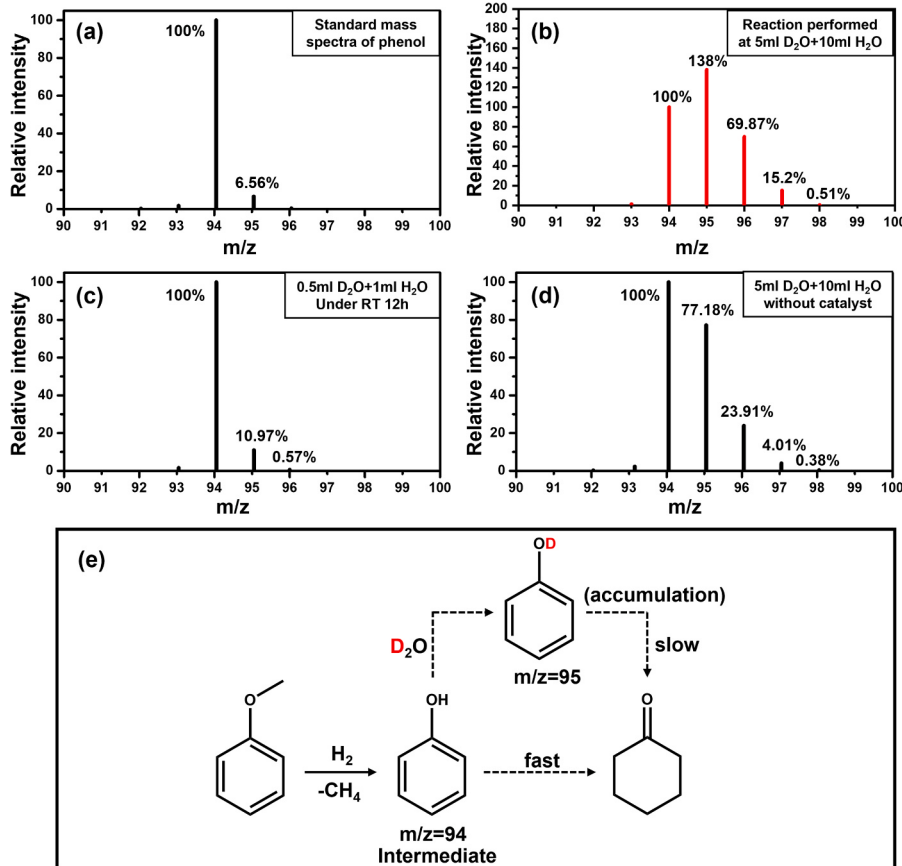


Fig. 6. Mass spectrum of phenol in isotope tracing experiment using D_2O . (a) standard mass spectra of phenol, (b) reaction performed at 5 ml $\text{D}_2\text{O} + 10 \text{ ml H}_2\text{O}$, reaction condition: 5.54 mmol anisole, 200 mg catalyst, 180 °C, 3 h, 2 MPa, (c) phenol is dissolved in 0.5 ml $\text{D}_2\text{O} + 1 \text{ ml H}_2\text{O}$ under RT for 12 h, and (d) reaction performed at 5 ml $\text{D}_2\text{O} + 10 \text{ ml H}_2\text{O}$, reaction condition: 5.54 mmol phenol, 180 °C, 3 h, 2 MPa, (e) proposed reaction pathway for the partial hydrogenation of anisole.

natural H-D exchange of phenol in D_2O . In the first experiment, phenol was dissolved in a solvent of 0.5 ml D_2O and 1 ml H_2O under room temperature (25°C) for 12 h (Fig. 6c). For another experiment, reaction under the same condition was performed without catalyst in 5 ml D_2O and 10 ml H_2O (Fig. 6d). The proportion of $m/z(95)$ to $m/z(94)$ was 10.97% and 77.18%, respectively, demonstrating there are indeed a very small portion of natural H-D exchange of phenol, but it is still much lower than that of 138% as shown in Fig. 6b. The accumulation of deuterium-phenol is attribute to the relatively lower reaction rate for further reaction compared with phenol, indicating that the phenol is an intermediate for partial hydrogenation of anisole (Fig. 6e). In other words, the hydrogenolysis of anisole to phenol is expected to be the first step of the reaction pathway.

In the similar style, Figure S11 shows the mass spectra of obtained cyclohexanone product by hydrogenation reaction using D_2O compared with the standard mass spectra of cyclohexanone, including the characteristic m/z of 55, 69 and 98 (Figure S11b). The deuterium-containing cyclohexanone is also founded in the product. Therefore, it is suggested that H_2O plays an important role to provide hydrogen for hydrogenation to produce cyclohexanone, which is in accordance with the result of solvent screening (Figure S7).

In order to explore the role of water in the selective hydrogenation of anisole, we further carried out H_2^{18}O isotope tracing experiments. The standard mass spectrum of cyclohexanone is shown in Fig. 7b. The peak of m/z (98) is assigned to the molecule peak of cyclohexanone, which is set as 100% as an intensity reference. The peak of m/z = 100 of ^{18}O -cyclohexanone only accounts for 0.38%, which is due to the natural abundance of ^{18}O . Then, a reaction was performed by using H_2^{18}O as part of the solvent (H_2^{18}O portion: 20%). However, it is found that the intensity of m/z = 100 increased to 16.70% (Fig. 7a). It shows that the oxygen atom of the product cyclohexanone comes from the oxygen atom in molecule water instead of the oxygen of the ether bond, which again indicates that water directly participates in the reaction in the selective hydrogenation of anisole. The oxygen atoms of phenol are still derived from ether bonds, but the oxygen atom in cyclohexanone is mainly from water (see Fig. 7c).

3.5. Discussion on reaction mechanism

Based on above spectroscopy studies and isotope tracing experiments, we can conclude that the single dispersed Pd is in cationic state coordinated by negative oxygen atoms in the micropores of ZSM-5. This type of configuration resembles the well-known classical Lewis pairs (CLPs).^[66] The Pd-O bond is similar to $\text{Pd}^{\delta+}\cdots\text{O}^{\delta-}$, where the H_2 can be activated by heterolytic cleavage.^[67,68] Hence, it's proposed that the

hydrogen molecules undergo a heterogeneous cleavage at Pd_1O_4 to form H^+ and H^- , and then H species are catalytically added to the reaction substrate [24,38,41,42,69]. This was confirmed in the D_2O isotope experiment (Figure S11). The production of multiple D substituted cyclohexanone is due to the exchange of D^+ in D_2O and H^+ generated by the decomposition of hydrogen at the single-atom Pd sites, which leads to D^+ participating in the catalytic hydrogenation reaction and the formation of multi-D substituted cyclohexanone. Nevertheless, the H-D exchange efficiencies of $\text{Pd}_1/\text{ZSM-5}$ and $\text{PdNP}/\text{ZSM-5}$ also suggest the distinct H_2 dissociation ability per Pd atoms. As shown in Figure S15, the HD signal (m/z = 3) intensities per surface Pd atoms demonstrate the single atom Pd sites in zeolite are active for H_2 dissociation. However, the site specific activity is lower than that of Pd atoms in the metallic PdNPs. This mediocre H_2 dissociation ability may be another factor to inhibit the over reduction of the product.

Hence, we propose a reaction path for the selective hydrogenation of anisole over $\text{Pd}_1/\text{ZSM-5}$ catalyst, as shown in Scheme 1. The metal center of $\text{Pd}_1/\text{ZSM-5}$ was unveiled by TEM (Fig. 1), DRIFT-CO (Figure S6) and XAS (Fig. 2), that is a palladium single atom anchored in the micropores of ZSM-5 with the configuration of Pd_1O_4 . Moreover, the substrate, anisole, can be adsorbed on the strong Brønsted acid sites of $\text{Pd}_1/\text{ZSM-5}$ (Fig. 5). Hence, the active center of $\text{Pd}_1/\text{ZSM-5}$ can be described as two series of adjacent monodispersed Pd sites and Brønsted acid sites, as shown in Scheme 1a. In addition, the isotope tracing experiment using D_2O implies phenol is the intermediate of reaction (Fig. 6). The first step of reaction is mainly hydrogenolysis of anisole into phenol on the active center (Supplementary Note 3). Hence, when anisole and hydrogen are introduced, the BAS adsorbs anisole while the hydrogen is dissociated into H^+ and H^- at the Pd_1O_4 sites simultaneously. Sequentially, the highly active H^- species transfer to anisole coupled with water and hydrogenate the methyl groups to form methane and leaves one phenol adsorbed on the BAS, as shown in Scheme 1b. Next, another two hydrogen molecules dissociate on the Pd_1O_4 sites and hydrogenate the benzene ring of adsorbed phenol to form cyclohex-2-en-1-yloxonium, as shown in Scheme 1e. The isotope tracing experiment using H_2^{18}O proves that the oxygen atom of cyclohexanone comes from H_2^{18}O instead of the original oxygen of aromatic ether (Fig. 7). Hence, the cyclohex-2-en-1-yloxonium is added to water to form the (2-hydroxycyclohexyl)-oxonium, as shown in Scheme 1f [70,71]. Since the original hydroxyl oxygen is adsorbed and activated by the BAS, this hydroxyl group is easily eliminated with the adjacent H atom to form H_3O^+ . Then the (2-hydroxycyclohexyl)-oxonium is converted to an enol before desorbing on the surface of the catalyst, and cyclohexanone is produced through tautomerism, as shown in Scheme 1g-h [9]. Finally, the acid center and the metal center decompose a molecule of water to

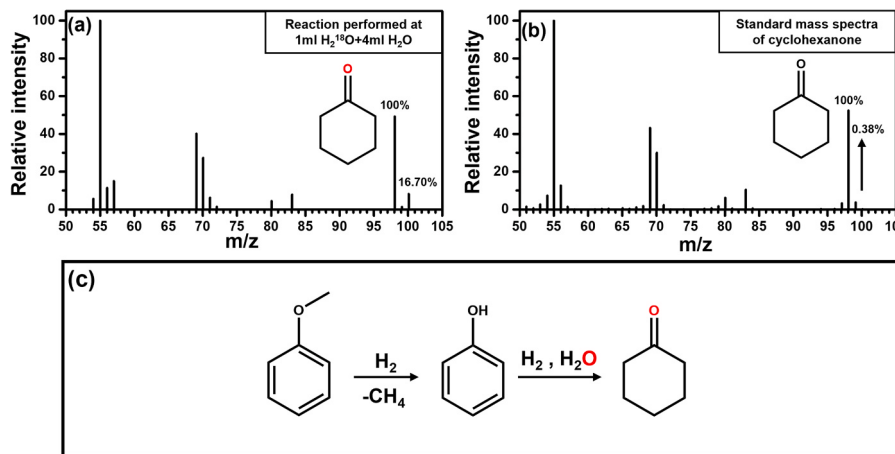
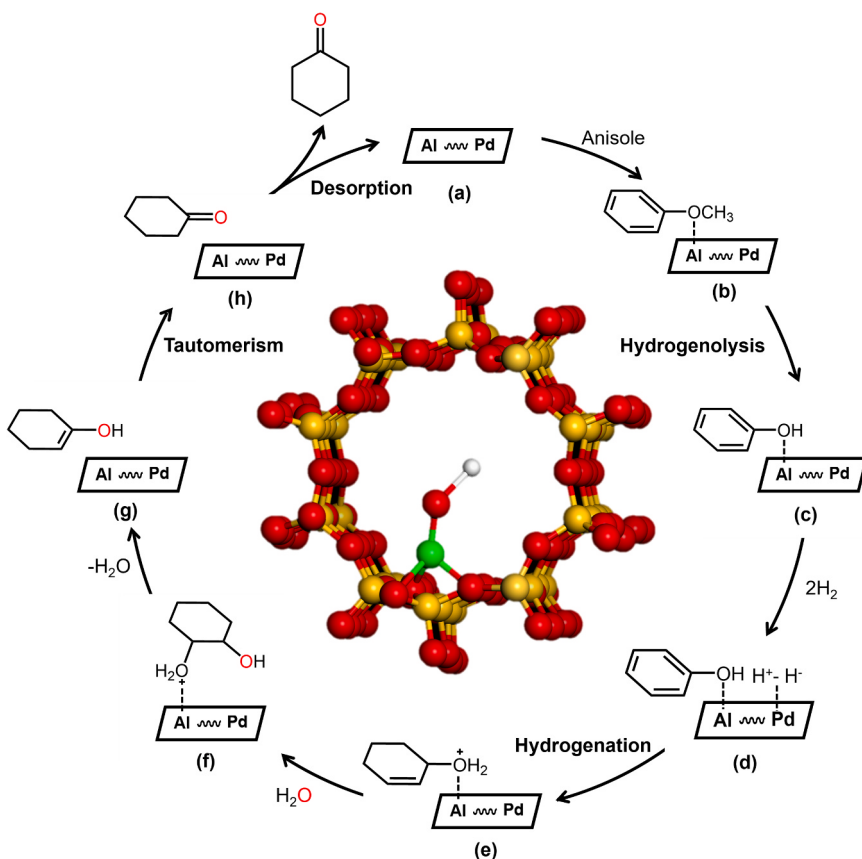


Fig. 7. Mass spectra of cyclohexanone in isotope tracing experiment using H_2^{18}O . (a) Mass spectrum of cyclohexanone obtained by reaction, Reaction condition: 5.54 mmol anisole, 100 mg catalyst, 1 ml H_2^{18}O + 4 ml H_2O , 180°C , 3 h, 2 MPa. (b) Standard mass spectrum of cyclohexanone, (c) proposed reaction pathway for the partial hydrogenation of anisole.



Scheme 1. The reaction pathway of partial hydrogenation of anisole to cyclohexanone.

restore the initial catalytic sites. This mechanism involved with water is different from the reported selective hydrogenation mechanism of anisole. The anisole was first hydrogenolysis into phenol and then hydrogenated to cyclohexanone. Overall, this water addition-elimination mechanism leads to the selective hydrogenation reaction of anisole can be carried out in the green solvent water and has a very high conversion rate and selectivity to cyclohexanone.

4. Conclusion

In summary, the $\text{Pd}_1/\text{ZSM-5}$ catalyst composed of two series of adjacent monodispersed acids and metal active sites has been successfully designed and applied for the partial hydrogenation of the biomass-derived molecule anisole to cyclohexanone. The synergistic effect of two active sites shows high activity and selectivity. Under $180\text{ }^\circ\text{C}$, 2 MPa of initial hydrogen pressure, the selectivity of cyclohexanone can reach $91.2 \pm 1.8\%$, while the turnover rate is as high as $400.8 \pm 30.1\text{ h}^{-1}$. The catalyst shows good reusability. The configuration of the single atomically dispersed Pd cation in the catalyst is Pd_1O_4 . The Brønsted acid sites serve as an important catalytic site for adsorbing and activating of anisole. Nevertheless, water not only acts as a solvent but also directly participates in the catalytic hydrogenation reaction of anisole. The unique water participated mechanism leads to the partial hydrogenation reaction of anisole which can only be carried out in water medium and has extremely high selectivity and conversion rate. Therefore, our work demonstrates a successful exploration to design single atom catalyst for sustainable production of high value chemicals.

CRediT authorship contribution statement

Kaiyang Xu: Investigation, Writing – original draft, Writing – review & editing, **Yu Chen:** Investigation, **Hua Yang:** Investigation, **Yuyan**

Gan: Investigation, **Lizhi Wu:** Formal analysis, Funding acquisition, **Li Tan:** Formal analysis, Funding acquisition, **Yihu Dai:** Investigation; **Yu Tang:** Supervision, Conceptualization, Writing – original draft, Writing – review & editing, Funding acquisition.

Declaration of Competing Interest

The authors declare the following financial interests/personal relationships which may be considered as potential competing interests: Yu Tang and Kaiyang Xu has patent #CN113019435B issued to Yu Tang, Kaiyang Xu, Zemin An.

Data availability

Data will be made available on request.

Acknowledgements

This work is supported by the National Natural Science Foundation of China (21902027, U19B2003 and 22172032); and Natural Science Foundation of Fujian Province (2020J01443, 2020J05121 and 2022J05110).

Appendix A. Supporting information

Supplementary data associated with this article can be found in the online version at [doi:10.1016/j.apcatb.2023.123244](https://doi.org/10.1016/j.apcatb.2023.123244).

References

[1] Y. Wang, J. Yao, H. Li, D. Su, M. Antonietti, Highly selective hydrogenation of phenol and derivatives over a $\text{Pd}@\text{Carbon nitride}$ catalyst in aqueous media, *J. Am. Chem. Soc.* 133 (2011) 2362–2365.

[2] H. Sun, F. Blatter, H. Frei, Cyclohexanone from cyclohexane and O₂ in a zeolite under visible light with complete selectivity, *J. Am. Chem. Soc.* 118 (1996) 6873–6879.

[3] H. Liu, T. Jiang, B. Han, S. Liang, Y. Zhou, Selective phenol hydrogenation to cyclohexanone over a dual supported Pd-lewis acid catalyst, *Science* 326 (2009) 1250–1252.

[4] J. He, Research progress in cyclohexanone synthesis by catalytic oxidation, *Synth. Fiber Ind.* 30 (2007) 43–46.

[5] L.X. Xu, C.H. He, M.Q. Zhu, K.J. Wu, Y.L. Lai, Surface stabilization of gold by sol-gel post-modification of alumina support with silica for cyclohexane oxidation, *Catal. Commun.* 9 (2008) 816–820.

[6] Y.Z. Chen, C.W. Liaw, L.I. Lee, Selective hydrogenation of phenol to cyclohexanone over palladium supported on calcined Mg/Al hydrotalcite, *Appl. Catal. A-Gen.* 177 (1999) 1–8.

[7] M.A. Ali, A. Abutaleb, An updated comprehensive literature review of phenol hydrogenation studies, *Catal. Lett.* 152 (2022) 1555–1581.

[8] J. Zhong, J. Chen, L. Chen, Selective hydrogenation of phenol and related derivatives, *Catal. Sci. Technol.* 4 (2014) 3555–3569.

[9] H. Chen, J. Sun, Selective hydrogenation of phenol for cyclohexanone: a review, *J. Ind. Eng. Chem.* 94 (2021) 78–91.

[10] X. Kong, Y. Gong, S. Mao, Y. Wang, Selective hydrogenation of phenol, *ChemNanoMat* 4 (2018) 432–450.

[11] K. Lee, Y. Jing, Y. Wang, N. Yan, A unified view on catalytic conversion of biomass and waste plastics, *Nat. Rev. Chem.* 6 (2022) 635–652.

[12] C. Li, X. Zhao, A. Wang, G.W. Huber, T. Zhang, Catalytic transformation of lignin for the production of chemicals and fuels, *Chem. Rev.* 115 (2015) 11559–11624.

[13] Z. Zhang, M. Liu, J. Song, H. Liu, Z. Xie, S. Liu, Q. Meng, P. Zhang, B. Han, Pd nanoparticles/polyoxometalate-ionic liquid composites on SiO₂ as multifunctional catalysts for efficient production of ketones from diaryl ethers, *Green. Chem.* 20 (2018) 4865–4869.

[14] C.A. Scaldaferrri, P. Warakunwit, V. Pasa, D.E. Resasco, C-O cleavage of diphenyl ether followed by C-C coupling reactions over hydrophobized Pd/HY catalysts, *Appl. Catal. B-Environ.* 259 (2019), 118081.

[15] F. Alshehri, C. Feral, K. Kirkwood, S.D. Jackson, Low temperature hydrogenation and hydrodeoxygenation of oxygen-substituted aromatics over Rh/silica: part 1: phenol, anisole and 4-methoxyphenol, *React. Kinet. Mech. Catal.* 128 (2019) 23–40.

[16] M. Wang, H. Shi, D.M. Camaioni, J.A. Lercher, Palladium-catalyzed hydrolytic cleavage of aromatic C-O bonds, *Angew. Chem. Int. Ed.* 56 (2017) 2110–2114.

[17] J. Schmid, M. Wang, O.Y. Gutierrez, R.M. Bullock, D.M. Camaioni, J.A. Lercher, Controlling reaction routes in noble-metal-catalyzed conversion of Aryl ethers, *Angew. Chem. Int. Ed.* 61 (2022), e202203172.

[18] L. Zhao, J.-P. Cao, Y.-L. Wei, W. Jiang, J.-X. Xie, C. Zhang, X.-Y. Zhao, M. Zhao, H.-C. Bai, Rational synthesis of palladium nanoparticles modified by phosphorous for the conversion of diphenyl ether to KA oil, *Appl. Catal. A-Gen.* 630 (2022), 118464.

[19] M. Zhao, L. Zhao, J.-P. Cao, W. Jiang, J.-X. Xie, C. Zhu, S.-Y. Wang, Y.-L. Wei, X.-Y. Zhao, H.-C. Bai, Water-involved tandem conversion of aryl ethers to alcohols over metal phosphide catalyst, *Chem. Eng. J.* 435 (2022), 134911.

[20] Q. Meng, M. Hou, H. Liu, J. Song, B. Han, Synthesis of ketones from biomass-derived feedstock, *Nat. Commun.* 8 (2017) 14190.

[21] S.K. Kaiser, Z. Chen, D.F. Akl, S. Mitchell, J. Perez-Ramirez, Single-atom catalysts across the periodict table, *Chem. Rev.* 120 (2020) 11703–11809.

[22] L. Liu, A. Corma, Metal catalysts for heterogeneous catalysis: from single atoms to nanoclusters and nanoparticles, *Chem. Rev.* 118 (2018) 4981–5079.

[23] Q. Sun, N. Wang, T. Zhang, R. Bai, A. Mayoral, P. Zhang, Q. Zhang, O. Terasaki, J. Yu, Zeolite-encaged single-atom rhodium catalysts: highly-efficient hydrogen generation and shape-selective tandem hydrogenation of nitroarenes, *Angew. Chem. Int. Ed.* 58 (2019) 18570–18576.

[24] L. Zhang, M. Zhou, A. Wang, T. Zhang, Selective hydrogenation over supported metal catalysts: from nanoparticles to single atoms, *Chem. Rev.* 120 (2020) 683–733.

[25] Z. Li, S. Ji, Y. Liu, X. Cao, S. Tian, Y. Chen, Z. Niu, Y. Li, Well-defined materials for heterogeneous catalysis: from nanoparticles to isolated single-atom sites, *Chem. Rev.* 120 (2020) 623–682.

[26] M. Babucci, A. Guntida, B.C. Gates, Atomically dispersed metals on well-defined supports including zeolites and metal-organic frameworks: structure, bonding, reactivity, and catalysis, *Chem. Rev.* 120 (2020) 11956–11985.

[27] W. Huang, S. Zhang, Y. Tang, Y. Li, N. Luan, Y. Li, J. Shan, D. Xiao, R. Gagne, A. I. Frenkel, F. Tao, Low-temperature transformation of methane to methanol on Pd₁O₄ single sites anchored on the internal surface of microporous silicate, *Angew. Chem. Int. Ed.* 55 (2016) 13441–13445.

[28] K. Khivantsev, N.R. Jaegers, L. Kovarik, J.C. Hanson, F. Tao, Y. Tang, X. Zhang, I. Z. Koleva, H.A. Aleksandrov, G.N. Vayssilov, Y. Wang, F. Gao, J. Szanyi, Achieving atomic dispersion of highly loaded transition metals in small-pore zeolite SSZ-13: high-capacity and high-efficiency low-temperature CO and passive NO_x adsorbers, *Angew. Chem. Int. Ed.* 57 (2018) 16672–16677.

[29] L. Wu, Z. Ren, Y. He, M. Yang, Y. Yu, Y. Liu, L. Tan, Y. Tang, Atomically dispersed Co²⁺ sites incorporated into a silicalite-1 zeolite framework as a high-performance and coking-resistant catalyst for propane nonoxidative dehydrogenation to propylene, *ACS Appl. Mater. Interfaces* 13 (2021) 48934–48948.

[30] Z. Yang, H. Li, H. Zhou, L. Wang, L. Wang, Q. Zhu, J. Xiao, X. Meng, J. Chen, F.-S. Xiao, Coking-resistant iron catalyst in ethane dehydrogenation achieved through siliceous zeolite modulation, *J. Am. Chem. Soc.* 142 (2020) 16429–16436.

[31] Y. Tang, Y. Li, V. Fung, D.-e Jiang, W. Huang, S. Zhang, Y. Iwasawa, T. Sakata, N. Luan, X. Zhang, A.I. Frenkel, F. Tao, Single rhodium atoms anchored in micropores for efficient transformation of methane under mild conditions, *Nat. Commun.* 9 (2018) 1231.

[32] Z. Jin, X. Yi, L. Wang, S. Xu, C. Wang, Q. Wu, L. Wang, A. Zheng, F.-S. Xiao, Metal-acid interfaces enveloped in zeolite crystals for cascade biomass hydrodeoxygenation, *Appl. Catal. B-Environ.* 254 (2019) 560–568.

[33] L. Wu, J. Wei, Y. Zhang, Y. He, X. Wang, H. Guo, Y. Tang, L. Tan, The selective hydrodeoxygenation of guaiacol to cyclohexanol over cobalt-modified TS-1 catalysts, *Microporous Mesoporous Mater.* 348 (2023), 112347.

[34] Y. Tang, S. Xu, Y. Dai, X. Yan, R. Li, L. Xiao, J. Fan, Solid phase metallurgy strategy to sub-5 nm Au-Pd and Ni-Pd bimetallic nanoparticles with controlled redox properties, *Chem. Commun.* 50 (2014) 213–215.

[35] N. Zheng, J. Fan, G.D. Stucky, One-step one-phase synthesis of monodisperse noble-metallir nanoparticles and their colloidal crystals, *J. Am. Chem. Soc.* 128 (2006) 6550–6551.

[36] B. Ravel, M. Newville, Athena, artemis, hephaestus: data analysis for X-ray absorption spectroscopy using IFEFFIT, *J. Synchrotron Radiat.* 12 (2005) 537–541.

[37] Q. Meng, H. Fan, H. Liu, H. Zhou, Z. He, Z. Jiang, T. Wu, B. Han, Efficient transformation of anisole into methylated phenols over high-silica HY zeolites under mild conditions, *Chemcatchem* 7 (2015) 2831–2835.

[38] W. Gao, S. Liu, G. Sun, C. Zhang, Y. Pan, Single-atom catalysts for hydrogen activation, *Small* (2023), 2300956.

[39] F. Wang, C.H. Li, L.D. Sun, C.H. Xu, J.F. Wang, J.C. Yu, C.H. Yan, Porous single-crystalline palladium nanoparticles with high catalytic activities, *Angew. Chem. Int. Ed.* 51 (2012) 4872–4876.

[40] Y. Li, U. Kanbur, J. Cui, G. Wang, T. Kobayashi, A.D. Sadow, L. Qi, Supported lanthanum borohydride catalyzes CH borylation inside zeolite micropores, *Angew. Chem. Int. Ed.* 61 (2022), e202117394.

[41] K. Khivantsev, N.R. Jaegers, I.Z. Koleva, H.A. Aleksandrov, L. Kovarik, M. Engelhard, F. Gao, Y. Wang, G.N. Vayssilov, J. Szanyi, Stabilization of super electrophilic Pd²⁺ cations in small-pore SSZ-13 zeolite, *J. Phys. Chem. C* 124 (2020) 309–321.

[42] N.R. Jaegers, K. Khivantsev, L. Kovarik, D.W. Klas, J.Z. Hu, Y. Wang, J. Szanyi, Catalytic activation of ethylene C-H bonds on uniform d(8) Ir(I) and Ni(II) cations in zeolites: toward molecular level understanding of ethylene polymerization on heterogeneous catalysts, *Catal. Sci. Technol.* 9 (2019) 6570–6576.

[43] X. Lu, C. Guo, M. Zhang, L. Leng, J.H. Horton, W. Wu, Z. Li, Rational design of palladium single-atoms and clusters supported on silicoaluminophosphate-31 by a photochemical route for chemoselective hydrodeoxygenation of vanillin, *Nano Res.* 14 (2021) 4347–4355.

[44] D. Wilson, M.A. Langell, XPS analysis of oleylamine/oleic acid capped Fe₃O₄ nanoparticles as a function of temperature, *Appl. Surf. Sci.* 303 (2014) 6–13.

[45] Q. Deng, H. Peng, Z. Yang, T. Wang, J. Wang, Z. Zeng, S. Dai, A one-pot synthesis of high-density biofuels through bifunctional mesoporous zeolite-encapsulated Pd catalysts, *Appl. Catal. B-Environ.* 337 (2023), 122982.

[46] Y. Tang, L. Ma, J. Dou, C.M. Andolina, Y. Li, H. Ma, S.D. House, X. Zhang, J. Yang, F. Tao, Transition of surface phase of cobalt oxide during CO oxidation, *Phys. Chem. Chem. Phys.* 20 (2018) 6440–6449.

[47] Y. Xu, Z. An, X. Yu, J. Yao, Q. Lv, H. Yang, Z. Lv, H. Guo, Q. Jiang, W. Liu, L. Wu, L. Tan, Y. Dai, Y. Tang, Enhanced catalytic stability and structural evolution of Rh-BN interface in dry reforming of methane under intensified CO₂ partial pressure, *J. Catal.* 427 (2023), 115094.

[48] G. Li, Y. Dai, Y. Yang, D.E. Resasco, Can we predict whether water will inhibit or enhance a given catalytic reaction, *Chem. Catal.* 1 (2021) 959–961.

[49] D.T. Bregante, A.M. Johnson, A.Y. Patel, E.Z. Ayla, M.J. Cordon, B.C. Bukowski, J. Greeley, R. Gounder, D.W. Flaherty, Cooperative effects between hydrophilic pores and solvents: catalytic consequences of hydrogen bonding on alkene epoxidation in zeolites, *J. Am. Chem. Soc.* 141 (2019) 7302–7319.

[50] G. Li, B. Wang, D.E. Resasco, Water-mediated heterogeneously catalyzed reactions, *ACS Catal.* 10 (2020) 1294–1309.

[51] Z. Zhao, R. Bababrik, W. Xue, Y. Li, N.M. Briggs, N. Dieu-Thy, U. Nguyen, S. P. Crossley, S. Wang, B. Wang, D.E. Resasco, Solvent-mediated charge separation drives alternative hydrogenation path of furanics in liquid water, *Nat. Catal.* 2 (2019) 431–436.

[52] Y. Dai, X. Gao, X. Chu, C. Jiang, Y. Yao, Z. Guo, C. Zhou, C. Wang, H. Wang, Y. Yang, On the role of water in selective hydrogenation of cinnamaldehyde to cinnamyl alcohol on PtFe catalysts, *J. Catal.* 364 (2018) 192–203.

[53] N. Pfreim, P.H. Hintermeier, S. Eckstein, S. Kim, Q. Liu, H. Shi, L. Milakovic, Y. Liu, G.L. Haller, E. Barath, Y. Liu, J.A. Lercher, Role of the ionic environment in enhancing the activity of reacting molecules in zeolite pores, *Science* 372 (2021) 952–957.

[54] G. Ertl, H. Knözinger, J. Weitkamp, *Handbook of heterogeneous catalysis*, VCH Weinheim (1997).

[55] H. Jin, R. Zhao, P. Cui, X. Liu, J. Yan, X. Yu, D. Ma, W. Song, C. Cao, Sabatier phenomenon in hydrogenation reactions induced by single-atom density, *J. Am. Chem. Soc.* 145 (2023) 12023–12032.

[56] H. Li, J. Liu, S. Xie, M. Qiao, W. Dai, Y. Lu, H. Li, Vesicle-assisted assembly of mesoporous Ce-doped Pd nanospheres with a hollow chamber and enhanced catalytic efficiency, *Adv. Funct. Mater.* 18 (2008) 3235–3241.

[57] G. Neri, A.M. Visco, A. Donato, C. Milone, M. Malentacchi, G. Gubitosa, Hydrogenation of phenol to cyclohexane over palladium and alkali-doped palladium catalysts, *Appl. Catal. A-Gen.* 110 (1994) 49–59.

[58] J.N. Shangguan, N. Pfreim, Y.H. Chin, Mechanistic details of C-O bond activation in and H-addition to guaiacol at water-Ru cluster interfaces, *J. Catal.* 370 (2019) 186–199.

[59] W.J. Balfour, The vibrational spectrum of anisole, *Spectrochim. Acta Part A Mol. Spectrosc.* 39 (1983) 795–800.

[60] A.S. Gemechu, L.J.H. Hoffmann, S. Marquardt, C.G. Eisenhardt, H. Baumgartel, R. Chelli, G. Cardini, S. Califano, The absorption spectrum of anisole and the anisole/CO₂ 1: 1-cluster. The influence of intermolecular interaction on intramolecular vibrations, *Z. für Phys. Chem.* 218 (2004) 123–153.

[61] R.S. da Silveira, A.M. de Oliveira, S.B.C. Pergher, V.T. da Silva, I.M. Baibich, Palladium and molybdenum mono and bimetallic catalysts on modernite for direct NO decomposition reaction, *Catal. Lett.* 129 (2009) 259–265.

[62] A.N. Pestryakov, V.V. Lunin, S. Fuentes, N. Bogdanchikova, A. Barrera, Influence of modifying additives on the electronic state of supported palladium, *Chem. Phys. Lett.* 367 (2003) 102–108.

[63] L.S.F. Feio, C.E. Hori, S. Damyanova, F.B. Noronha, W.H. Cassinelli, C.M. P. Marques, J.M.C. Bueno, The effect of ceria content on the properties of Pd/CeO₂/Al₂O₃ catalysts for steam reforming of methane, *Appl. Catal. A-Gen.* 316 (2007) 107–116.

[64] N. Li, X. Xing, J. Cheng, Z. Zhang, Z. Hao, Influence of oxygen and water content on the formation of polychlorinated organic by-products from catalytic degradation of 1,2-dichlorobenzene over a Pd/ZSM-5 catalyst, *J. Hazard. Mater.* 403 (2021), 123952.

[65] D.L. Gerrard, W.F. Maddams, P.J. Tucker, Solvent effects in u.v. absorption spectra. IV. Substituted phenols, anisole and phenetole, *Spectrochim. Acta A* 34 (1978) 1225–1230.

[66] Z.-Q. Huang, L.-P. Liu, S. Qi, S. Zhang, Y. Qu, C.-R. Chang, Understanding all-solid frustrated-lewis-pair sites on CeO₂ from theoretical perspectives, *ACS Catal.* 8 (2018) 546–554.

[67] X. Deng, B. Qin, R. Liu, X. Qin, W. Dai, G. Wu, N. Guan, D. Ma, L. Li, Zeolite-encaged isolated platinum ions enable heterolytic dihydrogen activation and selective hydrogenations, *J. Am. Chem. Soc.* 143 (2021) 20898–20906.

[68] Y. Chai, G. Wu, X. Liu, Y. Ren, W. Dai, C. Wang, Z. Xie, N. Guan, L. Li, Acetylene-selective hydrogenation catalyzed by cationic confined in zeolite, *J. Am. Chem. Soc.* 141 (2019) 9920–9927.

[69] P. Liu, Y. Zhao, R. Qin, S. Mo, G. Chen, L. Gu, D.M. Chevrier, P. Zhang, Q. Guo, D. Zang, B. Wu, G. Fu, N. Zheng, Photochemical route for synthesizing atomically dispersed palladium catalysts, *Science* 352 (2016) 797–801.

[70] A.M. Robinson, J.E. Hensley, J.W. Medlin, Bifunctional catalysts for upgrading of biomass-derived oxygenates: a review, *ACS Catal.* 6 (2016) 5026–5043.

[71] C. Zhao, J. He, A.A. Lemonidou, X. Li, J.A. Lercher, Aqueous-phase hydrodeoxygenation of bio-derived phenols to cycloalkanes, *J. Catal.* 280 (2011) 8–16.